

Folliculin Controls Lung Alveolar Enlargement and Epithelial Cell Survival through E-Cadherin, LKB1, and AMPK

Elena A. Goncharova,^{1,5} Dmitry A. Goncharov,^{1,5} Melane L. James,¹ Elena N. Atochina-Vasserman,¹ Victoria Stepanova,² Seung-Beom Hong,¹ Hua Li,¹ Linda Gonzales,⁴ Masaya Baba,⁷ W. Marston Linehan,⁷ Andrew J. Gow,⁶ Susan Margulies,³ Susan Guttentag,⁴ Laura S. Schmidt,^{7,8} and Vera P. Krymskaya^{1,*}

¹Pulmonary, Allergy and Critical Care Division, Airways Biology Initiative, Department of Medicine, Perelman School of Medicine, Philadelphia, PA 19104, USA

²Department of Pathology and Laboratory Medicine, Perelman School of Medicine, Philadelphia, PA 19104, USA

³Department of Bioengineering, School of Engineering and Applied Science, University of Pennsylvania, Philadelphia, PA 19104, USA

⁴Children's Hospital of Philadelphia, Philadelphia, PA 19104, USA

⁵Vascular Medicine Institute, University of Pittsburgh, Pittsburgh, PA 15261, USA

⁶Department of Pharmacology & Toxicology, Rutgers University, Piscataway, NJ 08854, USA

⁷Urologic Oncology Branch, National Cancer Institute, Bethesda, MD 20892, USA

⁸Basic Science Program, Leidos Biomedical Research, Inc., Frederick National Laboratory for Cancer Research, Frederick, MD 20892, USA

*Correspondence: krymskay@mail.med.upenn.edu

<http://dx.doi.org/10.1016/j.celrep.2014.03.025>

This is an open access article under the CC BY-NC-ND license (<http://creativecommons.org/licenses/by-nc-nd/3.0/>).

SUMMARY

Spontaneous pneumothoraces due to lung cyst rupture afflict patients with the rare disease Birt-Hogg-Dubé (BHD) syndrome, which is caused by mutations of the tumor suppressor gene *folliculin* (*FLCN*). The underlying mechanism of the lung manifestations in BHD is unclear. We show that BHD lungs exhibit increased alveolar epithelial cell apoptosis and that *Fln* deletion in mouse lung epithelium leads to cell apoptosis, alveolar enlargement, and an impairment of both epithelial barrier and overall lung function. We find that *Fln*-null epithelial cell apoptosis is the result of impaired AMPK activation and increased cleaved caspase-3. AMPK activator LKB1 and E-cadherin are downregulated by *Fln* loss and restored by its expression. Correspondingly, *Fln*-null cell survival is rescued by the AMPK activator AICAR or constitutively active AMPK. AICAR also improves lung condition of *Fln*^{fl/fl}; *SP-C-Cre* mice. Our data suggest that lung cysts in BHD may result from an underlying defect in alveolar epithelial cell survival, attributable to FLCN regulation of the E-cadherin-LKB1-AMPK axis.

INTRODUCTION

Birt-Hogg-Dubé (BHD) syndrome is a rare autosomal-dominant disorder that affects lung, skin, and kidney (Birt et al., 1977). In the lung, 80%–100% of patients with BHD develop multiple thin-wall cysts without evidence of neoplasia, inflammation, or fibrosis (Gupta et al., 2013). Cyst rupture and lung collapse cause spontaneous and recurrent pneumothoraces (Gupta et al.,

2013). In contrast to lung, *FLCN* mutations in the kidney result in bilateral multifocal renal cell carcinomas (Schmidt, 2004), and in hair follicles result in hamartomas (fibrofolliculomas). The mechanism by which the loss of FLCN promotes the development of cysts but not neoplasia is unknown.

Genetic mapping in families with BHD identified the *Folliculin* (*FLCN*) gene locus (Nickerson et al., 2002; Schmidt et al., 2001). Loss of heterozygosity in BHD lesions supports a tumor suppressor function for *FLCN* (Vocke et al., 2005). Homozygous *Fln*^{-/-} mice are embryonically lethal, and heterozygous *Fln*^{+/-} mice develop kidney tumors without lung pathology (Hasumi et al., 2009). In *Drosophila* and yeast, FLCN is involved in the mammalian target of rapamycin signaling pathway and in energy metabolism (Liu et al., 2013; van Slegtenhorst et al., 2007). Inactivation of FLCN induces mitochondrial gene expression (Hasumi et al., 2012). Studies also suggest crosstalk of FLCN with the master energy sensor AMP-activated protein kinase (AMPK) via FLCN-interacting proteins FNIP1 and FNIP2 (Baba et al., 2006; Hasumi et al., 2008; Takagi et al., 2008). How these signaling events relate to FLCN function in normal lung or in pulmonary cyst development in BHD is unknown.

The prevailing hypothesis used to explain the development of emphysematous alveolar enlargement and cyst formation in lung diseases involves an imbalance between matrix degrading matrix metalloproteinases (MMPs) and their endogenous inhibitors the tissue inhibitor of metalloproteinases (Shapiro and Ingenito, 2005; Suki et al., 2003). The notion, however, that alveolar epithelial cell (AEC) apoptosis is a primary event in the pathogenesis of alveolar enlargement related to lung injury has become an area of significant interest (Henson and Tuder, 2008; Mouded et al., 2009). The FLCN-dependent mechanism of cystic lung enlargement in BHD and the functional significance of *FLCN* inactivation in the lung remain uncharacterized.

Cell-cell and cell-matrix interactions are critical components of epithelial cell survival, and disruption of these interactions

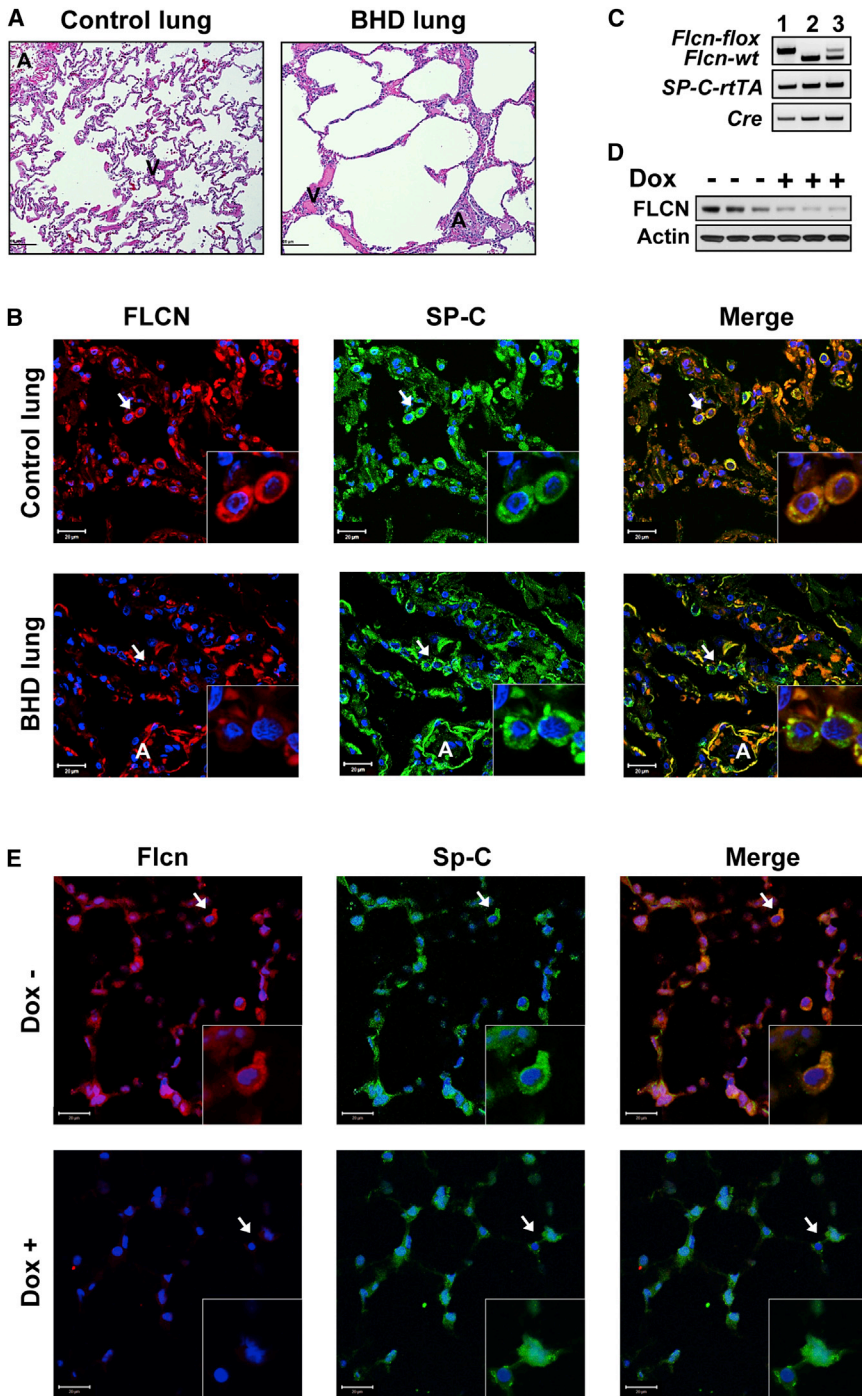


Figure 1. Lung Histology and FLCN and SP-C Immunostaining

(A) H&E staining of normal human lung (Control) (n = 3) and BHD lung (n = 4). A, conducting airways; V, blood vessels.

(B) FLCN-positive (red) AECs (SP-C, green) are seen in normal human lung (n = 3), but not in BHD (n = 4) lungs. DAPI (blue) stains nuclei. Arrows indicate FLCN immunostaining colocalized with SP-C expression in AECs in control lungs, but not in lungs from patients with BHD.

(C) Genotyping of homozygous *Flcn*^{fl/fl}:*SP-C-Cre* (1), *Flcn*^{WT/WT}:*SP-C-Cre* (2), and heterozygous *Flcn*^{WT/fl}:*SP-C-Cre* mice (3).

(D) Flcn levels in whole-lung lysates from *Flcn*^{fl/fl}:*SP-C-Cre* mice on Dox (Dox+) for 6 weeks (n = 3) or a regular (Dox-) diet (n = 3).

(E) Loss of Flcn (red) in lung AECs (SP-C, green) in *Flcn*^{fl/fl}:*SP-C-Cre* mice treated as in (D). Arrows indicate FLCN immunostaining colocalized with SP-C expression in *Flcn*^{fl/fl}:*SP-C-Cre* mice on a Dox-, but not on a Dox+, diet.

Scale bars, 20 μ M. See also Figure S1.

2013). E-cadherin regulates the localization of LKB1 to epithelial cell junctions, and loss of E-cadherin impairs LKB1-mediated AMPK activation (Sebbagh et al., 2009).

These observations raise the possibility that FLCN might be involved in the regulation of AMPK signaling in AECs and that inactivating mutation of *FLCN* might impair epithelial cell junctions and cell survival. In this study, we investigate this possibility with cell-type-specific inducible *Flcn* deletion in mouse lung epithelium and with *FLCN*-null human and mouse epithelial cell systems.

RESULTS

Loss of *Flcn* in Lung Epithelium Results in Increased Alveoli

Hematoxylin and eosin (H&E) staining of control human lung reveals typical lung structure (Figure 1A, left). In contrast, lungs from patients with BHD showed irregular and disrupted lung parenchyma (Figure 1A, right). Healthy alveoli are lined with type I and the surfactant protein

often leads to caspase-mediated apoptosis (Frisch and Screaton, 2001). AMPK is required for cell survival and for the maintenance of epithelial cell junctions (Hardie, 2011; Lee et al., 2008; Liu et al., 2010; Zheng and Cantley, 2007). AMPK activity is regulated through phosphorylation by LKB1 (Hardie, 2011), a tumor suppressor gene associated with 30% of lung cancers (Makowski and Hayes, 2008). LKB1 controls the maturation of apical junctions in human bronchial epithelial cells (Xu et al.,

C (SP-C)-expressing type II AECs (Figures S1A and S1B), a renewable population of progenitors in these distal airspaces. We used coimmunostaining to determine FLCN expression in human lung from healthy controls and subjects with BHD. In control lung, FLCN staining colocalizes with SP-C expression in AECs (Figure 1B, top). Coimmunostaining of lung tissue from patients with BHD detects very little FLCN in alveolar SP-C-positive cells (Figure 1B, bottom).

To evaluate the role of FLCN in lung, we selectively deleted *Fln* in SP-C-expressing alveolar epithelial type II cells (*Fln^{fl/fl}:SP-C-Cre*) by crossing *Fln^{fl/fl}* mice (Baba et al., 2008) with *SP-C-rtTA/tetO-Cre* (line 2) mice (Perl et al., 2009) (Figure S1C) to generate *Fln^{fl/fl}:SP-C-Cre* mice with inducible *Fln* deletion in SP-C-expressing cells by a dietary supplementation with doxycycline (Dox) starting at 6 weeks of age. Under this SP-C promoter, Cre expression is targeted to the AECs in alveoli and peripheral bronchioles (Perl et al., 2009). *Fln^{fl/fl}:SP-C-Cre* mice do not exhibit perinatal lethality or reduced survival, and weights were comparable across *Fln^{fl/fl}:SP-C-Cre*, *Fln^{WT/WT}:SP-C-Cre*, and *Fln^{fl/WT}:SP-C-Cre* genotypes. The Dox diet did not affect mouse survival or weights and did not cause pulmonary distress. Genotyping, immunoblotting, and coimmunostaining analyses of *Fln^{fl/fl}:SP-C-Cre* mouse lungs confirmed *Fln* deletion with the Dox diet (Figures 1C–1E, bottom). Immunoblotting (Figure 1D, Dox+ lanes) shows residual *Fln* expression in non-SP-C-expressing cells in whole-lung lysates. Importantly, inflation-fixed lungs from epithelial-specific *Fln*-deleted mice exhibited alveolar enlargement (Figure 2A).

Morphometric lung measurements of mean linear intercept (MLI) and mean alveolar airspace area (MAAA) are significantly larger in lungs of epithelial-specific *Fln*-deleted mice than in lungs of *Fln*-expressing *Fln^{fl/fl}:SP-C-Cre* mice (Figures 2B, 2C, and S1D–S1F). However, the overall structure and organization of the lungs are nearly normal. The lung alveoli of *Fln^{WT/WT}:SP-C-Cre* or *Fln^{fl/WT}:SP-C-Cre* mice on a regular or Dox-supplemental diet appear unchanged and comparable with lung alveoli of *Fln^{fl/fl}:SP-C-Cre* mice on a regular diet.

FLCN Is Required for Postnatal Lung Alveolarization

To determine the role of FLCN during lung development, female *Fln^{fl/fl}:SP-C-Cre* mice were placed on a Dox-supplemented diet starting at embryonic day 0.5 (E0.5). Newborn pups were viable and appeared normal with no increased perinatal lethality. However, postnatal pups with lung epithelial-specific *Fln* deletion exhibited larger alveoli compared to pups with *Fln*-expressing lung epithelium (Figures 2D–2F). These data show developmental changes induced by FLCN deletion in lung epithelium and suggest a role for FLCN in branching morphogenesis of the lung.

FLCN Regulates Lung Function

Morphological changes that resemble emphysema, such as alveolar enlargement, contribute to a decline in lung elastic recoil and pulmonary function. Lung function tests of adult *Fln^{fl/fl}:SP-C-Cre* mice fed Dox for 6 weeks were markedly abnormal compared to age- and gender-matched littermates maintained on a regular diet. Decreased airway elastance and resistance and increased dynamic compliance were observed in *Fln^{fl/fl}:SP-C-Cre* mice with *Fln* deletion in lung epithelium compared to *Fln*-expressing controls (Figure 2G).

To determine whether *Fln* loss in other lung epithelial cells might also impair lung function, we generated *Fln^{fl/fl}:CCSP-Cre* mice with targeted *Fln* deletion in lung epithelial cells expressing Clara cell secretory protein (CCSP) (Perl et al., 2009) (Figures S1G and S1H). CCSP-expressing lung epithelial cells localize in alveoli and bronchioles (Perl et al., 2009). *Fln* deletion in

Fln^{fl/fl}:CCSP-Cre mice did not result in differences in the lung function (Figure S1I) compared to age- and gender-matched controls. These results demonstrate that lung parenchyma and function are affected by *Fln* deletion specifically in AECs expressing SP-C, and alveolar epithelium is vulnerable to loss of FLCN during early lung development as well as in the mature lung.

FLCN Is Required for AEC Survival In Vivo

To evaluate whether apoptosis plays a role in airspace enlargement in BHD, control and BHD human lung tissues were immunostained with cleaved caspase-3 antibody. As seen in Figure 2H, apoptotic SP-C-positive cells were detected in BHD lung, but not in control human lung. AECs positive for activated caspase-3 were identified in lungs of *Fln^{fl/fl}:SP-C-Cre* mice maintained on a Dox diet compared to age- and gender-matched littermates maintained on a regular diet (Figure 2I). Terminal deoxynucleotidyl transferase dUTP nick end labeling (TUNEL) staining to assess DNA fragmentation was also detected in human BHD lungs and mouse lungs with deleted FLCN (Figure S2). Importantly, TUNEL staining colocalizes with SP-C immunostaining (Figure S2C).

FLCN Downregulates LKB1 and Controls AMPK Activity

Because our results show that FLCN regulates AEC survival in vivo, we sought to identify the mechanism. AMPK activation is required to maintain epithelial cell-cell junctions, thus preserving epithelial barriers and promoting cell survival (Hardie, 2011). To determine whether FLCN deficiency affects AMPK activation, we used the *FLCN*-null human epithelial renal tumor cell line UOK257 derived from the kidney tumor of a patient with BHD, and UOK257 cells with stably re-expressed FLCN (UOK257-2) used as a control (Baba et al., 2006).

AMPK is phosphorylated on Thr172 by LKB1 under conditions of stress, such as nutrient deprivation. Serum depletion of FLCN-expressing UOK257-2 cells for 24 and 48 hr resulted in time-dependent AMPK phosphorylation at Thr172 (Figure 3A). Phosphorylation of acetyl-coenzyme A-carboxylase (ACC) by activated AMPK also increased in a time-dependent manner in FLCN-expressing UOK257-2 cells. In contrast, *FLCN*-null cells exhibited reduced AMPK activation and ACC phosphorylation compared to *FLCN*-expressing UOK257-2 cells (Figure 3A). Importantly, serum deprivation also increased cleaved caspase-3 in *FLCN*-null UOK257 cells, but not in *FLCN*-expressing UOK257-2 cells (Figure 3B).

To further examine the effect of FLCN loss on AMPK activation in lung epithelial cells, we isolated primary mouse AECs from lungs of *Fln^{fl/fl}:SP-C-Cre* mice. Cells were treated with either an empty, replication-defective adenovirus or a replication-defective adenovirus expressing Cre-recombinase to delete *Fln* (Figure 4A). Immunostaining with antibody against T1 α , an AEC marker (Ramirez et al., 2003), showed T1 α expression in primary mouse AECs from *Fln^{fl/fl}:SP-C-Cre* mice (Figure S3). AMPK(Thr172) phosphorylation was significantly decreased in *Fln*-null AECs in contrast to *Fln*-expressing AECs (Figure 4A). Small interfering RNA (siRNA)-induced *Fln* knockdown in mouse epithelial NMuMG cells also significantly decreased

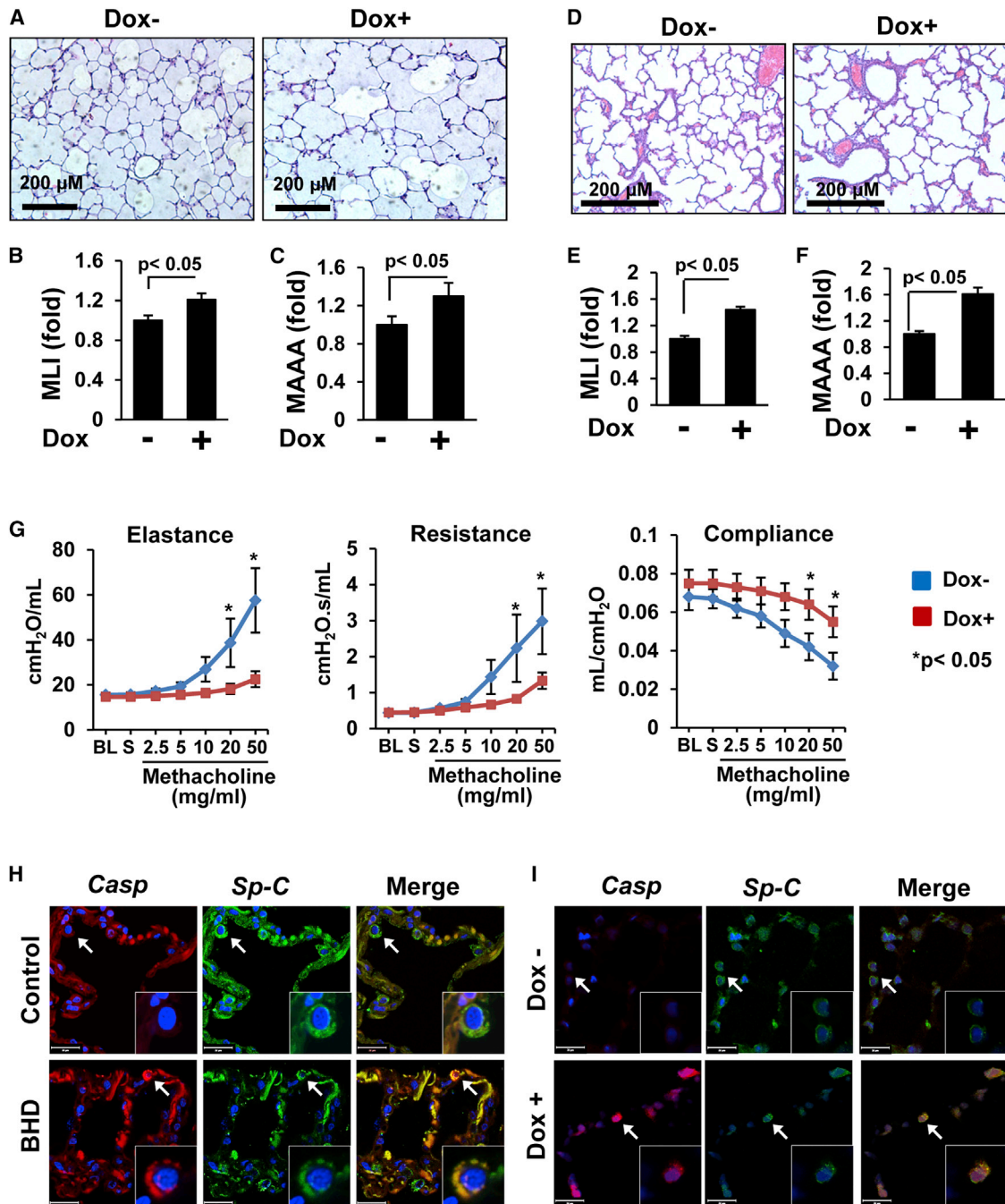


Figure 2. Loss of FLCN Increases Pulmonary Alveoli, Impairs Lung Function, and Induces AEC Apoptosis

(A–C) Flcn loss results in alveolar enlargement in *Flcn^{fl/fl};SP-C-Cre* mice treated as in Figure 1D.

(D–F) Enlarged alveoli in pups with FLCN deletion in lung epithelium.

In (B), (C), (E), and (F), the mean is shown; error bars represent SE (n > 3). Data for Dox– mice are taken as 1-fold.

(G) FLCN deletion in *Flcn^{fl/fl};SP-C-Cre* mice impairs lung function (n = 8 per group). BL, baseline; S, saline.

(H) Cleaved caspase-3-positive (red) cells in lung epithelium (SP-C, green) of BHD lung (n = 5), but not in control (n = 3) lung. Arrows indicate cleaved caspase-3 immunostaining of SP-C-positive cells in lungs from patients with BHD, but not in control lungs. Scale bars, 20 μ M.

(I) Loss of Flcn in lung epithelium (SP-C, green) results in AEC apoptosis (red) in lung from *Flcn^{fl/fl};SP-C-Cre* mice treated as in Figure 1D (n = 3 per group). Arrows indicate cleaved caspase-3 immunostaining of SP-C-positive cells in *Flcn^{fl/fl};SP-C-Cre* mice on a Dox+, but not on a Dox–, diet. Scale bars, 20 μ M.

See also Figure S2.

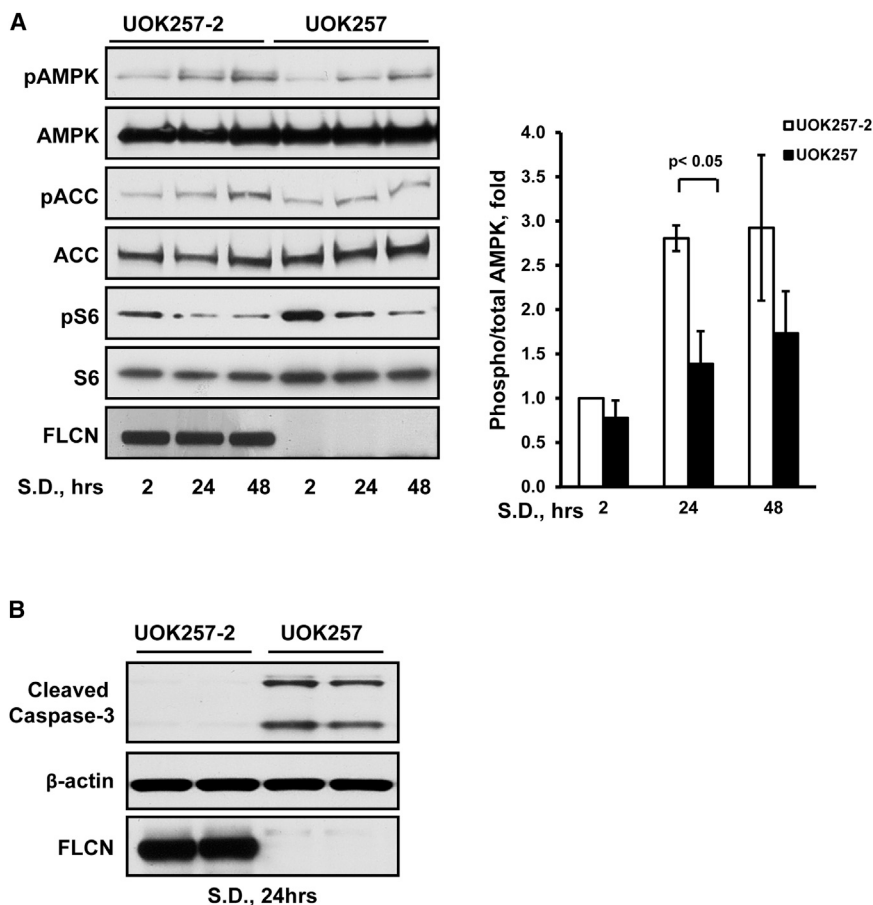


Figure 3. FLCN Loss Impairs AMPK Activation and Upregulates Cleaved Caspase-3

(A) *FLCN*-null UOK257 and *FLCN*-expressing UOK257-2 epithelial cells were serum deprived (S.D.) in Dulbecco's modified Eagle's medium supplemented with 0.1% BSA. Data are mean \pm SE (n = 3).

(B) Energy depletion of *FLCN*-null UOK257 cells upregulates cleaved caspase-3.

decreased in the absence of *Flcn* expression (Figures 5A–5C). Immunostaining also showed marked reduction of E-cadherin in the adherens junctions of cellular membranes (Figure 5D, top; Figures S4A and S4C). ZO-1 staining at tight junctions, however, appeared unchanged by *Flcn* deletion (Figure 5D, bottom; Figures S4B and S4C). Thus, *FLCN* has a specific effect on E-cadherin expression and localization to adherens junctions.

To further determine *FLCN*'s role in regulating E-cadherin, we used *TSC2*-null kidney epithelial cells, which have decreased membrane localization of E-cadherin (Figure 5E) (Barnes et al., 2010; Kleymenova et al., 2001). Transient transfection of *TSC2*-null cells with myc-tagged *FLCN* (Figure 5F) increased E-cadherin membrane localization, which was statistically significant (Figure 5G).

These data further suggest that *FLCN* may play a role in regulation of E-cadherin.

Increased *FLCN*-Null Epithelial Cell Permeability and Apoptosis

Epithelial cell barriers and permeability depend on the preservation of adherens and tight junctions (Frisch and Screaton, 2001). Our data show reduced E-cadherin localization in the *FLCN*-null cellular membrane, which might affect adherens junctions. Hence, we examined whether *FLCN* is required for the maintenance of cell permeability. Primary AECs isolated from lungs of *Flcn*^{fl/fl} mice were treated with empty adenovirus or Cre-recombinase-expressing adenovirus followed by a cell permeability assay using BODIPY-conjugated ouabain (DiPaolo and Margulies, 2012). Loss of *Flcn* resulted in increased permeability of primary AECs (Figure 5H) compared to cells expressing *Flcn*. In addition, loss of *Flcn* was associated with elevated cleaved caspase-3 levels and an increased number of cells with DNA fragmentation detected by TUNEL assay (Figures 5I–5K). These data demonstrate that *FLCN* is required for the maintenance of epithelial barrier integrity and AEC survival.

Similarly, mouse epithelial NMuMG cells transfected with siRNA *Flcn* exhibited decreased membrane localization of E-cadherin (Figures 6A and S5A). si*Flcn* also significantly decreased protein levels (Figure S5B) and *cdh1* (E-cadherin)

AMPK(Thr172) phosphorylation compared to cells transfected with control siRNA (Figure 4B).

We next examined LKB1 levels in cells deficient for *FLCN* because LKB1 activates AMPK via phosphorylation at Thr172-AMPK (Hardie, 2011). LKB1 levels were reduced in primary AECs after *Flcn* deletion (Figure 4A). LKB1 levels were also markedly decreased in NMuMG cells with *Flcn* knockdown induced by siRNA (Figure 4B). To further determine whether LKB1 expression is regulated by *FLCN*, *FLCN*-null UOK257 cells were transduced with replication-defective adenovirus expressing *FLCN*. *FLCN* re-expression in *FLCN*-null UOK257 cells significantly increased LKB1 levels (Figure 4C). Cellular fractionation showed significantly increased LKB1 levels induced by *FLCN* expression not only in cytosol but also in the membrane fraction (Figure 4C), confirming membrane localization of LKB1 (Sebbagh et al., 2009; Xu et al., 2013). These data suggest that *FLCN* regulates the cellular level and localization of LKB1.

Regulation of E-Cadherin by *FLCN*

Evidence demonstrates that E-cadherin regulates membrane localization of LKB1, which is critical for AMPK activation (Sebbagh et al., 2009). Therefore, we determined whether *Flcn* deletion in primary AECs would affect E-cadherin expression and/or localization. E-cadherin is significantly

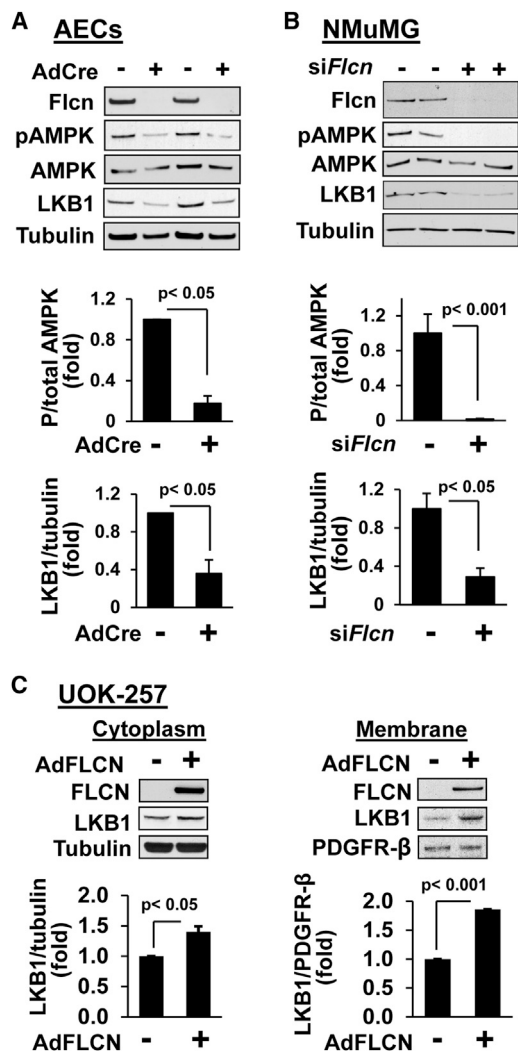


Figure 4. FLCN Regulates LKB1 Levels and AMPK Phosphorylation
 (A) Primary lung AECs from *Flcn*^{fl/fl} mice were infected with control (–) or Cre-recombinase-expressing adenovirus (AdCre,+) followed by immunoblot analysis. See also Figure S3.
 (B) Immunoblot analyses of mouse epithelial NMuMG cells transfected with *Flcn* siRNA (*siFlcn*) or control scrambled siRNA (–).
 (C) Re-expression of FLCN in human *FLCN*-null UOK-257 cells increases membrane localization of LKB1.
 Top, representative images. Bottom, statistical analyses. Protein ratio for control cells was taken as 1-fold. Data are mean ± SE (n = 3).

and *stk11* (LKB1) gene expression (Figures S5D and S5F). Furthermore, in cells transfected with *siFlcn*, E-cadherin does not maintain its multimeric structure as demonstrated by the presence of lower molecular weight staining under native conditions (Figure S5C), in contrast to no differences in LKB1 multimeric structure (Figure S5E) detected by native gel electrophoresis with equal loading of E-cadherin or LKB1 proteins.

Loss of *Flcn* in NMuMG cells also reduced transepithelial resistance (TER) (Figure 6B), another measure of increased

cell permeability (Zheng and Cantley, 2007). We could not use TER to measure the permeability of primary AECs because they grow on the Matrigel-coated plates, which impede TER measurements. Finally, *Flcn* knockdown in NMuMG cells also increased cleaved caspase-3 levels (Figure 6C) and apoptosis (Figure 6D). Analysis of apoptotic gene expression using RT² Profiler PCR Arrays (SABiosciences; QIAGEN) revealed pro-apoptotic gene upregulation and decreased expression of prosurvival genes by *Flcn* knockdown (Figures S6A–S6C). *Flcn*-dependent downregulation of prosurvival *Bcl-2* gene was further confirmed by decreased levels of *Bcl-2* protein levels (Figure S6D). Collectively, our data show that FLCN regulates membrane localization of E-cadherin, protein, and gene expression, maintains epithelial barrier function, and preserves epithelial cell survival.

AICAR and Constitutively Active AMPK Rescue FLCN-Deficient Cell Survival

Flcn knockdown visibly changes epithelial cell morphology with disruption of the cell monolayer (Figure 6E). To evaluate the role of AMPK in FLCN-deficient cell survival, mouse epithelial NMuMG cells were transfected with *siFlcn* and then treated with 5-aminoimidazole-4-carboxamide riboside (AICAR), a cell-permeable precursor of AMP that activates AMPK (Figure 6G). Treatment with AICAR reversed *Flcn*-induced disruption of epithelial cell morphology (Figure 6E). AICAR treatment also significantly reduced *Flcn*-induced DNA fragmentation (Figure 6H) and epithelial cell death (Figure 6I). Similar results were seen upon transduction with adenovirus expressing the constitutively active AMPK (AdAMPK-CA) (Figure 6F) of NMuMG cells after *Flcn* knockdown. Expression of constitutively active AMPK markedly improved *Flcn*-deficient cell morphology (Figure 6E), reduced DNA fragmentation (Figure 6H), and rescued epithelial cell survival (Figure 6I). These results demonstrate that the kinase activity of AMPK is required for cell survival in the absence of FLCN.

AICAR Improves Alveolar Surface Tension in *Flcn*^{fl/fl}:SP-C-Cre Mice

Our in vitro and in vivo data show that FLCN controls AEC survival. Alveolar type II cells are the only cells capable of manufacturing and secreting phospholipids into alveoli to reduce surface tension and support alveolar inflation at low lung volumes. We therefore measured surface tension and phospholipid composition obtained from bronchoalveolar lavage (BAL) of *Flcn*^{fl/fl}:SP-C-Cre mice on a regular or Dox-supplemented diet. Total phospholipids measured in large aggregate (LA) fractions of BAL from mice with *Flcn* deletion in lung epithelium were reduced compared to control mice (Figure 7A). In addition, we measured surface tension of LA phospholipids by a capillary surfactometer (Guttentag et al., 2005). The capillary surfactometer measures the ability of airflow to progress through a fluid-filled capillary. The capillary openness, as a percentage of capillary diameter, is inversely related to the surface tension of the fluid in the capillary. LA phospholipids from Dox-treated *Flcn*^{fl/fl}:SP-C-Cre mice exhibited increased surface tension compared to untreated littermates, as evidenced by reduced capillary openness (Figure 7B). Importantly,

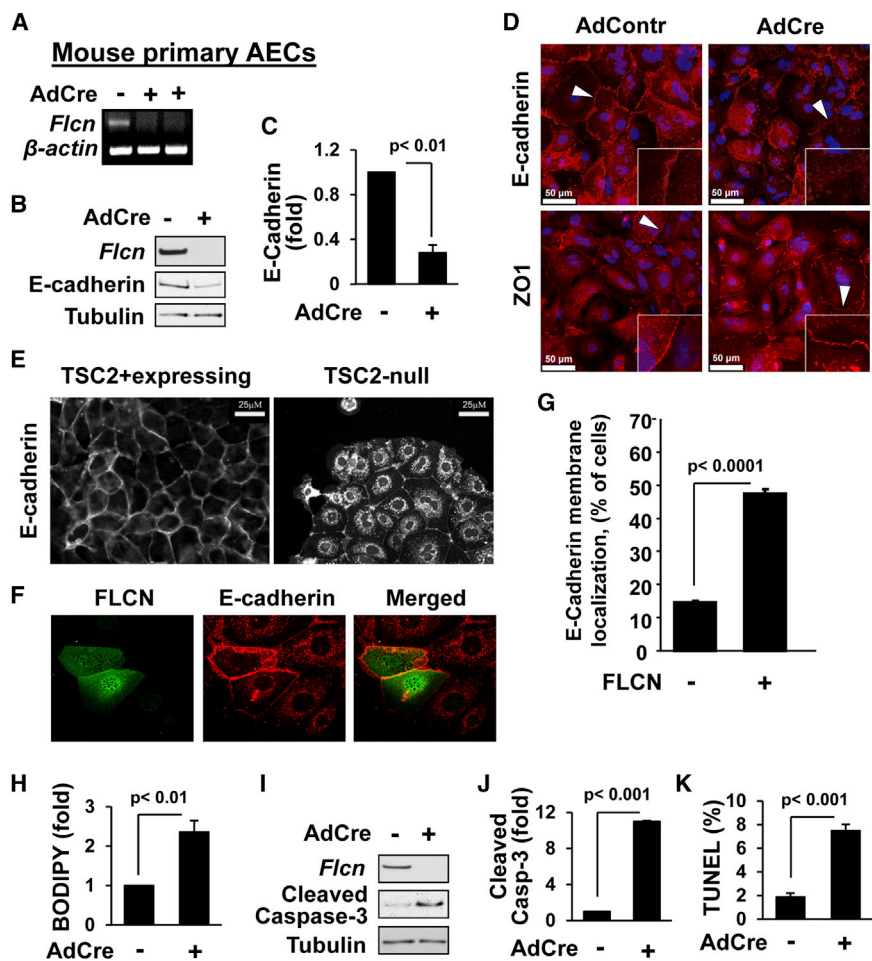


Figure 5. *Flcn* Loss Reduces E-Cadherin Levels, Increases Cellular Permeability, and Promotes Apoptosis of Primary Mouse Lung AECs

(A–C) AdCre-induced *Flcn* deletion in AECs from *Flcn^{fl/fl}* mice was detected by RT-PCR (A) and immunoblot (B) with statistical analysis (C). E-cadherin/tubulin ratio for control cells is taken as 1-fold.

(D) Loss of *Flcn* in AECs downregulates membrane localization of E-Cadherin (red, top), but not ZO1 (red, bottom) (as shown in arrowheads). DAPI (blue) stains nuclei.

See also Figure S4.

(E) Cytoplasmic E-cadherin localization in TSC2-null epithelial cells.

(F and G) FLCN expression (green) results in membrane localization of E-cadherin (red) in TSC2-null cells (F). Data (G) represent percentage (%) of cells; ≥ 60 cells/condition (F).

(H) *Flcn* deletion increases lung AEC permeability. Cell permeability in control is taken as 1-fold.

(I and J) *Flcn* deletion in lung AECs upregulates cleaved caspase-3.

(K) *Flcn* deletion in AECs results in DNA fragmentation. Number of TUNEL-positive cells to total number of cells is taken as 100%. Data are mean \pm SE ($n > 3$).

AICAR treatment improved phospholipid content and the surface tension of LA from Dox-treated *Flcn^{fl/fl}:SP-C-Cre* mice (Figures 7A and 7B). There was a trend toward improved AEC survival, morphology, MLI, and MAAA in Dox-treated *Flcn^{fl/fl}:SP-C-Cre* mice maintained on Dox and treated with AICAR compared to control mice also treated with AICAR (Figures 7C and 7E–7G, respectively). Thus, *Flcn* deletion in lung epithelium induces a physiologically significant aberration in surface tension of alveolar phospholipids that is stabilized by AICAR treatment.

AICAR Suppresses Inflammation and MMP Levels

Increased inflammation and proteolytic degradation of extracellular matrix components such as basement membrane or interstitial stroma are pathological changes characteristic of emphysema. To test whether loss of *Flcn* was associated with increased inflammation, we examined the BAL fluid for inflammatory cell influx. After 2 weeks on a Dox diet, *Flcn^{fl/fl}:SP-C-Cre* mice had increased numbers of total BAL cells compared with mice on a regular diet that was further increased by 6 weeks on Dox (Figures S6 and 7D). Importantly, Dox-treated *Flcn^{fl/fl}:SP-C-Cre* mice treated with AICAR exhibited decreased inflammatory cell influx (Figure 7D).

We examined the proinflammatory cytokine profile of BAL from Dox-treated *Flcn^{fl/fl}:SP-C-Cre* mice and untreated littermates to determine whether loss of *FLCN* alters cytokine expression. We found marked elevations in interleukin-6 (IL-6) and macrophage chemotactic protein-1 (MCP-1) in *Flcn^{fl/fl}:SP-C-Cre* mice on Dox compared to untreated littermates (Figures 7H and 7I). There were no significant differences between control mice and mice with *Flcn* deletion in AECs in the levels of eotaxin, granulocyte-macrophage colony-stimulating factor, interferon γ , tumor necrosis factor α , IL-10, IL-13, IL-1 β , keratinocyte chemoattractant, transforming growth factor β 1, vascular endothelial growth factor, and macrophage inflammatory protein 1 α (data not shown). Moreover, AICAR treatment lowered levels of IL-6 and MCP-1 in BAL fluid of mice with *Flcn* knockout.

MMPs represent a family of structurally and functionally related enzymes responsible for the proteolytic degradation of extracellular matrix and have been mechanistically linked with progressive pulmonary emphysema and chronic inflammation. BAL from Dox-treated *Flcn^{fl/fl}:SP-C-Cre* mice demonstrated significant elevations of MMP-3 and MMP-9 compared to untreated mice (Figures 7J and 7K). Furthermore, treatment with AICAR lowered MMP-3 and MMP-9 levels to levels comparable to control mice (Figures 7J and 7K). Collectively, in vivo experiments demonstrate that *Flcn* inactivation in lung AECs of *Flcn^{fl/fl}:SP-C-Cre* mice evokes inflammatory response and upregulation of MMP-3 and MMP-9 in a manner that is reversible with exogenous AMPK activation by AICAR.

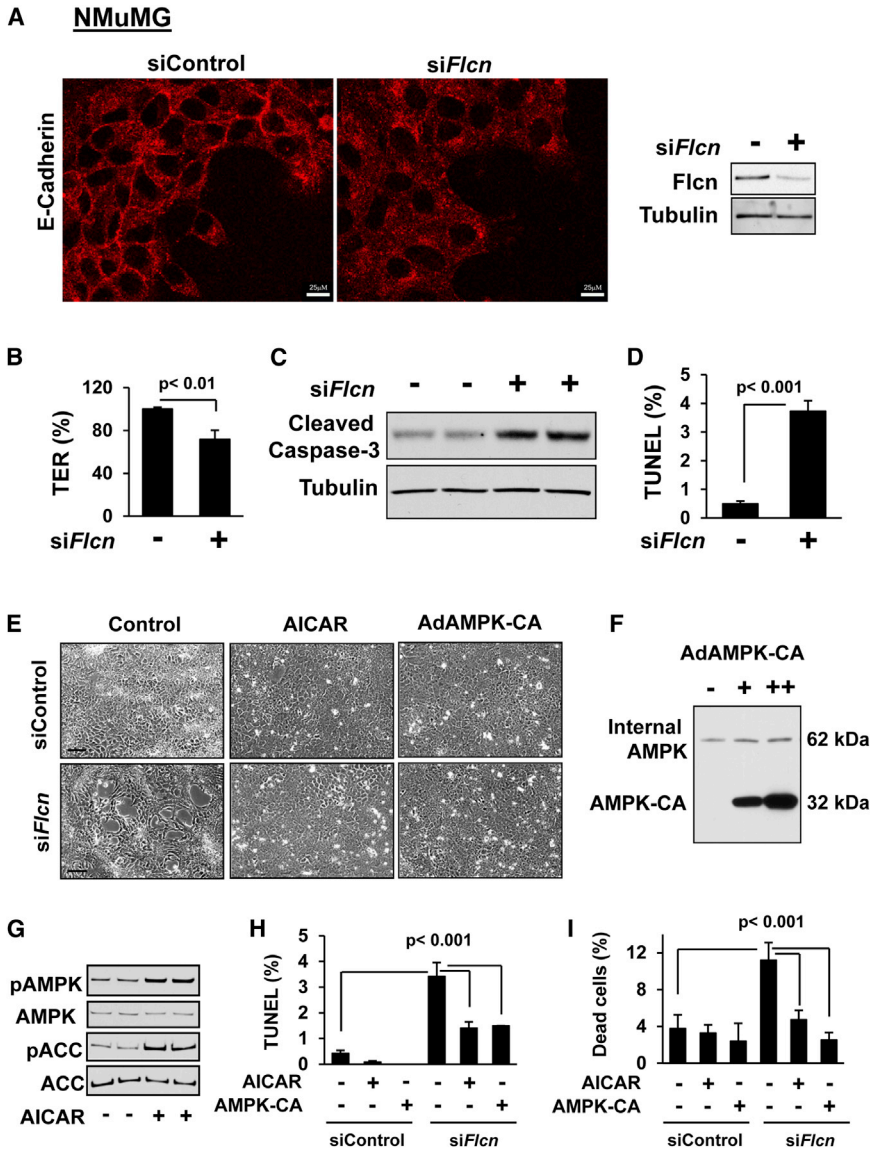


Figure 6. Increased *Flcn*-Null Epithelial Cell Apoptosis Is Rescued by AICAR and Constitutively Active AMPK

(A) *Flcn* knockdown downregulates membrane localization of E-cadherin (red). See also Figures S5 and S6.

(B) *Flcn* knockdown decreases TER. TER of siContra-transfected NMuMG cells was taken as 100%.

(C) Cleaved caspase-3 is upregulated by si*Flcn*. (D) *Flcn* knockdown induces DNA fragmentation (TUNEL assay) of NMuMG cells.

(E) AICAR and constitutively active AMPK (AMPK-CA) rescue disruption of epithelial cell morphology caused by si*Flcn*. Cells were treated either with 100 mM AICAR or diluent, or were infected with AdAMPK-CA or control adenovirus. Scale bars, 100 μ M.

(F and G) Expression of AMPK-CA (F) and AICAR-induced AMPK and ACC (G) phosphorylation in epithelial NMuMG cells.

(H and I) DNA fragmentation (H) and epithelial cell death (I) induced by *Flcn* loss are rescued by AICAR and AMPK-CA. Data represent percentage of TUNEL-positive (H) or dead (I) cells per total number of cells taken as 100%. Contr, control. Data are mean \pm SE (n = 3).

pulmonary disease (COPD), pulmonary lymphangioleiomyomatosis (LAM), pulmonary Langerhans cell histiocytosis (PLCH), lymphocytic interstitial pneumonia (LIP), follicular bronchiolitis, light-chain deposition disease, Sjögren's syndrome, and amyloidosis (Gupta et al., 2013). It is becoming increasingly clear that the mechanisms underlying the development of emphysematous changes in the lung are more complex than simply an imbalance of proteolysis and antiproteolysis. Together, our data provide additional supportive evidence

DISCUSSION

The present study identifies FLCN as a regulator of lung homeostasis and advances our understanding of the pathophysiology of emphysema. This study details the cellular and molecular mechanisms by which FLCN contributes to lung epithelial cell survival, thereby maintaining alveolar surface tension through maintenance of phospholipid production. As such, loss of FLCN leads to loss of epithelial cells with resultant reduction in phospholipid production that contributes to the lung changes associated with BHD (Figure 7L). Furthermore, we show that FLCN maintains epithelial cell junctions and survival in an AMPK-dependent fashion by regulating membrane localization of E-cadherin and LKB1 (Figure 7L).

The abnormal enlargement of airspaces is a major pathological manifestation of many common and rare lung diseases, including emphysema, cystic fibrosis, chronic obstructive

for the complex pathophysiology of emphysematous alveolar enlargement by showing that FLCN supports cell survival and influences the cytokine and MMP milieu in ways that might contribute to lung cyst formation with loss of FLCN in BHD. These insights into the role of FLCN may serve as a foundation for novel therapeutic approaches for BHD and other emphysematous lung diseases.

This study establishes that FLCN plays an important physiological role in regulating AEC survival and alveolar integrity. We demonstrate the importance of FLCN for AEC apoptosis in vivo and in vitro using *Flcn^{fl/fl}:SP-C-Cre* mice, by examining both lung tissue and isolated AECs. It is intriguing that *Flcn* loss in an immortalized mouse embryonic stem cell line resulted in transcriptional downregulation of proapoptotic protein Bim (Cash et al., 2011). Elucidating a more direct role for *Flcn* intersecting with apoptotic pathways will be possible in the future with our cell and mouse models.

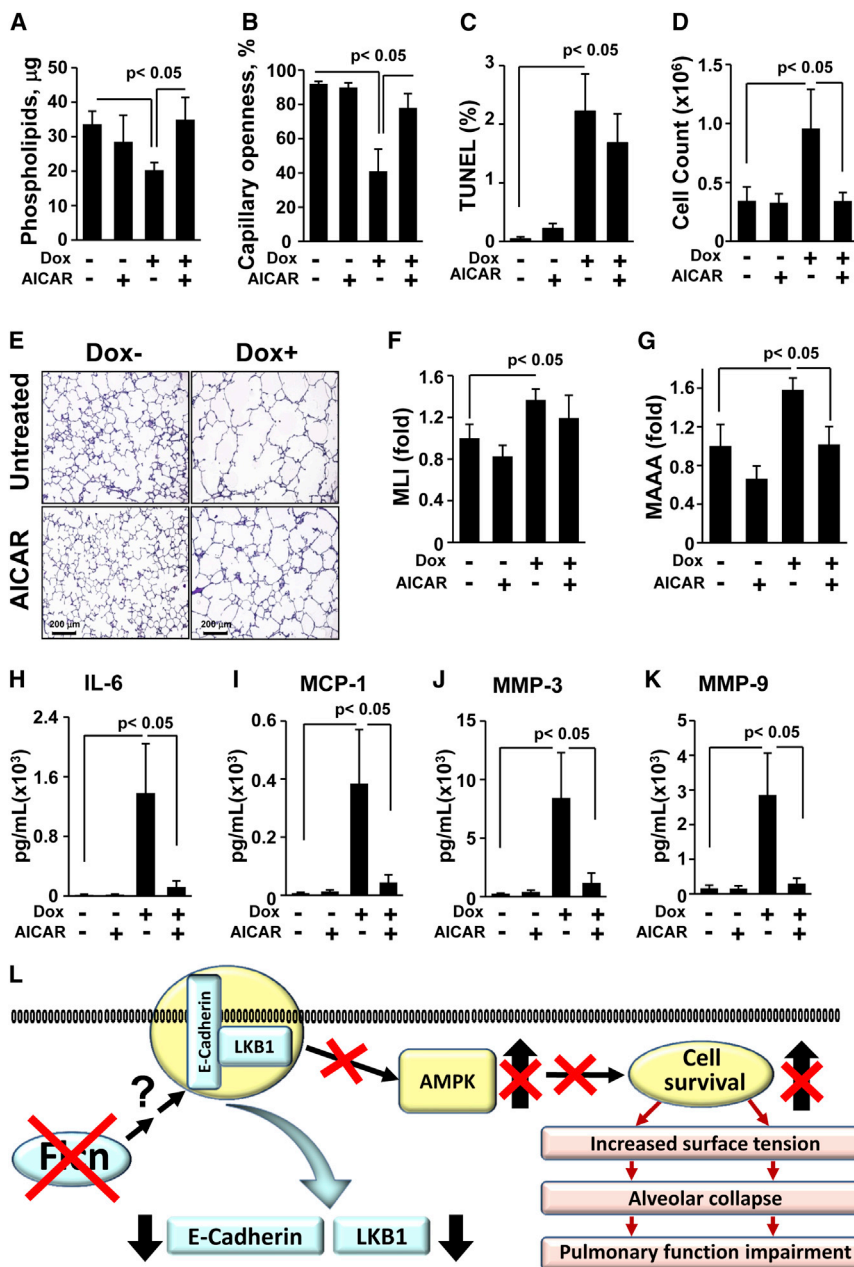


Figure 7. AICAR Improves Lung Homeostasis of *Flcn*^{fl/fl};*SP-C-Cre* Mice with *Flcn* Deletion in Lung Epithelium

(A) Abnormalities in pulmonary phospholipids in BAL resulting from *Flcn* deficiency are restored by AICAR. *Flcn*^{fl/fl};*SP-C-Cre* mice on Dox⁻ or Dox⁺ were treated with AICAR or diluent for 6 weeks. (B) *Flcn*-induced impairment of surfactant surface tension is rescued by AICAR.

(C) *Flcn* loss induces DNA fragmentation of AECs. Number of TUNEL-positive cells to total number of cells was taken as 100%. (D) AICAR normalizes increased inflammatory cell influx.

(E) H&E staining of *Flcn*^{fl/fl};*SP-C-Cre* mouse lungs on Dox⁻ or Dox⁺ treated with AICAR as in (A).

(F and G) Morphometric analyses of *Flcn*^{fl/fl};*SP-C-Cre* mouse lungs treated as in (A). The mean is shown; error bars represent SE (n > 3). Data for Dox⁻ mice are taken as 1-fold. (H and I) AICAR inhibits IL-6 (H) and MCP-1 (I) increased by *Flcn* loss.

(J and K) Upregulation of MMP-3 and MMP-9 induced by *Flcn* loss in lung epithelium treated as in (A) is abrogated by AICAR.

(L) A proposed model for the role of FLCN in lung alveolar homeostasis. *FLCN* mutations in lung epithelium downregulate membrane localization of E-cadherin and LKB1, which impairs AMPK activation. This model proposes that FLCN plays an important physiological function to control AEC survival and maintains alveolar surface tension. Loss of FLCN results in alveolar collapse and impairment of lung function.

See also Figure S7. Data in (A)–(K) are represented as mean \pm SEM from two independent experiments (n = 5–7).

Our data suggest that FLCN promotes survival of AECs through this E-cadherin/LKB1/AMPK axis. Our data also suggest that FLCN functions upstream of AMPK. Loss of FLCN affects assembly of adherens junctions via downregulation of E-cadherin levels while having little effect on ZO1 levels in tight junctions. Importantly, disruption of the epithelial monolayer and apoptosis caused by FLCN loss were prevented by either molecular

or pharmacological AMPK activation. Together with published studies, our data suggest that FLCN is required for E-cadherin-dependent epithelial cell-cell junctions, impairment of LKB1-AMPK signaling, and caspase-dependent apoptosis of lung AECs, the initial component of alveolar airspace enlargement. Further studies will provide detailed mechanisms of how FLCN regulates E-cadherin and LKB1 expressions.

One consequence of altered AEC survival is the loss of an important source of pulmonary phospholipids. Phospholipids play an important role in the maintenance of alveolar stability through the respiratory cycle, so it is perhaps not surprising that apoptosis-induced airspace enlargement is associated

Our studies clearly demonstrate that the prosurvival role is mediated through AMPK (Figure 7L). The prosurvival role of AMPK in epithelial cells is well established, especially as related to the maintenance of epithelial contacts and polarity (Zhang et al., 2006; Zheng and Cantley, 2007). Phosphorylation of AMPK by tumor suppressor LKB1 increases AMPK activity (Jansen et al., 2009). This requires the localization of LKB1 to E-cadherin at adherens junctions (Sebbagh et al., 2009). Evidence suggesting a role for AMPK in microtubule formation via CLIP-170 (Nakano et al., 2010), which also has a role in E-cadherin localization (Barnes, 2010), provides a reinforcing loop of E-cadherin/LKB1/AMPK regulation of apical polarity.

Our data suggest that FLCN promotes survival of AECs through this E-cadherin/LKB1/AMPK axis. Our data also suggest that FLCN functions upstream of AMPK. Loss of FLCN affects assembly of adherens junctions via downregulation of E-cadherin levels while having little effect on ZO1 levels in tight junctions. Importantly, disruption of the epithelial monolayer and apoptosis caused by FLCN loss were prevented by either molecular or pharmacological AMPK activation. Together with published studies, our data suggest that FLCN is required for E-cadherin-dependent epithelial cell-cell junctions, impairment of LKB1-AMPK signaling, and caspase-dependent apoptosis of lung AECs, the initial component of alveolar airspace enlargement. Further studies will provide detailed mechanisms of how FLCN regulates E-cadherin and LKB1 expressions.

One consequence of altered AEC survival is the loss of an important source of pulmonary phospholipids. Phospholipids play an important role in the maintenance of alveolar stability through the respiratory cycle, so it is perhaps not surprising that apoptosis-induced airspace enlargement is associated

with increased alveolar surface tension, and alveolar instability and collapse (Moudeed et al., 2009). However, this raises an important therapeutic possibility, specifically the potential for exogenous phospholipid therapy to mitigate the effects of AEC loss. Although exogenous phospholipid therapy for unintubated patients is currently unfeasible due to issues of delivery, novel delivery modalities or therapies targeting increased production of phospholipid by the remaining epithelial cell population are attractive options for the future.

The loss of FLCN also evokes an inflammatory response associated with local production of inflammatory cytokines and MMPs. Further studies will determine whether this is due to an epithelial injury response, or whether FLCN itself signals an anti-inflammatory pathway.

FLCN acts through an AMPK-mediated pathway that can be resurrected by exogenous activation of AMPK. AICAR, an AMPK activator, reverses many of the pathologic changes in the *Fln^{fl/fl}:SP-C-Cre* mice with *Fln* deletion limited to lung AECs. Importantly, AICAR rescues those features of *Fln* loss that are critical to the pathophysiology of lung cysts, specifically mitigating inflammation and MMP expression that propagate local alveolar damage and enhancing phospholipid production to stabilize airspace inflation. Although AMPK-dependent suppression of MMP-9 has been previously reported by Hwang and Jeong (2010) and Morizane et al. (2011), our data provide an attractive mechanism for a feedforward cycle of epithelial cell destabilization with loss of FLCN followed by further local destruction by enhanced MMP production. Further studies are needed to establish the mechanism(s) whereby impaired AMPK signaling increases MMP expression.

Rescue by AICAR does not reverse the structural changes due to FLCN loss. It does not rule out the possibility that AMPK agonists may have a role in prevention or that they may be useful to stop or slow the progression of existing emphysema.

There are several limitations of our studies. First, *Fln* deletion in *Fln^{fl/fl}:SP-C-Cre* mice does not precisely phenocopy lung changes in patients with BHD. Patients with BHD exhibit loss of alveoli and lung cyst development predominantly localized to the lower regions of the lung (Gupta et al., 2013). The differences between our mouse model and human patients may be due to either the restricted knockout of *Fln* in epithelial cells only or the expression of nonnull mutations of FLCN in patients with BHD. Despite these limitations, our data demonstrate the key role of FLCN in the maintenance of normal lung parenchyma architecture and physiology, and a well-defined mechanism whereby FLCN, acting through E-cadherin, LKB1, and AMPK, has a critical role in regulating the assembly of epithelial cell junctions.

EXPERIMENTAL PROCEDURES

The Human Lung Tissue

Control human lung tissues from three subjects were obtained from the National Disease Research Interchange, and the human BHD tissue samples from four patients with BHD were obtained from the NIH under approved protocols.

Animals

Fln^{fl/fl}:SP-C-Cre mice were generated by crossing *Fln^{fl/fl}* mice (Baba et al., 2008) with *SP-C-rtTA/tetO-Cre* (line 2) mice (Perl et al., 2009). *Fln^{fl/fl}:CCSP-C-Cre* mice were generated by crossing *Fln^{fl/fl}* mice with *CCSP-rtTA/tetO-Cre* mice (line 2) (Perl et al., 2009). Genotyping was performed as described (Baba et al., 2008). Six-week-old male *Fln^{fl/fl}:SP-C-Cre* or *Fln^{fl/fl}:CCSP-C-Cre* mice were transferred on chow supplemented with 2.5% Dox (Dox+) or maintained on a regular chow (Dox-) for 3 or 6 weeks. Treatment with 500 mg/kg AICAR was performed daily by intraperitoneal injections for 6 weeks in mice on Dox- or Dox+ diet.

Lung function was measured on a computerized FlexiVent System (SCIREQ) (Haczku et al., 2002). For morphological analyses, lungs were inflated at constant 25 cm H₂O pressure with 1:1 optimal cutting temperature/PBS or low-melting agarose in PBS for approximately 8 min (Goncharova et al., 2012). Each experimental group included a minimum of five animals per condition. Experiments to determine the effects of *Fln* loss on alveoli space enlargement were performed three times, and experiments with treatment by AICAR were performed twice. All animal procedures were performed according to a protocol approved by the University of Pennsylvania IACUC.

BAL Analyses

BAL fluid was collected by lavaging the lung with 1 ml of sterile saline to a total of 5 ml. Recovered BAL was centrifuged 400 × *g* for 10 min at 4°C, then cell pellet was resuspended in 1 ml PBS for total cell count. Cell-free BAL supernatants were separated by centrifugation at 20,000 × *g* for 60 min at 4°C into LA and small-aggregate (SA) phospholipid fractions. Surface tension was determined by measuring capillary openness with a capillary surfactometer (Calmia Medical) (Guttentag et al., 2005). Briefly, 0.5 μl of 1 mg/ml LA fraction was deposited into the glass capillary and compressed for 120 s, resulting in a cyclic extrusion from the narrow end of the capillary permitting airflow and capillary patency. Dysfunctional phospholipids exhibit decreased capillary patency that is inversely correlated with the surface tension. A microprocessor calculates the percentage of the 120 s period that the capillary is open to free airflow. Each sample was analyzed in triplicate. Cytokine and MMPs were determined in the cell-free BAL by SearchLight Multiplex ELISA at Aushon Biosystems.

Morphometry

Images of lung tissue sections stained with H&E were acquired with a Nikon Eclipse 80i microscope under 100× magnification. Ten randomly selected fields per slide from three nonserial sections were analyzed. Image-Pro Plus 6.2 software (Media Cybernetics) was used to measure the MAAA and MLI. Airway, vascular structures, and histological mechanical artifacts were eliminated from the analysis.

Immunohistochemical, immunocytochemical, and immunoblot analyses were performed as described (Goncharova et al., 2011). Immunostaining was visualized with a Leica SP5 X or Zeiss LSM 700 confocal microscope or a Nikon Eclipse TE2000-E microscope equipped with an Evolution QE1 digital video camera under appropriate filters. Protein levels were analyzed by optical density with Gel-Pro Analyzer software.

Cell Culture

AECs were isolated from 2-week-old *Fln^{fl/fl}* mice as described (Atochina-Vaserman et al., 2011). Mouse lungs were inflated in situ via tracheal cannulation with dispase. Dissected lobes were digested in modified Eagle's medium plus DNase I. The mixed cells were filtered, and fibroblasts were removed from the suspension by three successive adherence steps on plastic. Negative selection was used to purify epithelial cells from macrophages and other blood cells using magnetic beads (DynaMouse T Cell Negative Isolation Kit #114.13D). Cells were plated in HITES medium (prepared in Ham's F12 plus 15 mM HEPES, 0.8 mM CaCl₂, hydrocortisone, and β-estradiol) plus 10% fetal calf serum (FCS) on coverslips coated with 10% Matrigel (BD Biosciences) for immunofluorescence staining. Serum was added for 48 hr to facilitate adherence and was then removed to minimize overgrowth of any remaining fibroblasts. Human UOK-257 and UOK257-2 cell lines (Hong et al., 2010) and TSC2-null kidney epithelial cells from an Eker rat were prepared as described

by Kleymenova et al. (2001); mouse epithelial NMuMG cells were purchased from the American Type Culture Collection.

Flcn siRNA was from Dharmacon, and scrambled siRNA was from Santa Cruz Biotechnology. Transfection was performed using Effectene or RNAiFect reagents (QIAGEN). Infection with AdCre or AdFLCN adenovirus was described (Goncharova et al., 2004).

BODIPY Permeability Assay

The assay was performed as described (DiPaolo and Margulies, 2012). Briefly, 2 μ m BODIPY-ouabain (Invitrogen) was added to AECs for 1 hr. Then BODIPY-ouabain fluorescence was visualized using a green emission filter. Fluorescence was measured on four separate fields per well, and three wells were measured per condition. All measurements were normalized to values from cells infected with control adenovirus.

TER Measurements

TER was measured in confluent NMuMG cells, grown on electric cell substrate impedance-sensing (ECIS) 8W1E plates, then subjected to an elevated voltage pulse of 40 kHz frequency, 3.5 V amplitude for 30 s (Taliaferro-Smith et al., 2009).

Data Analysis

Data points from individual assays represent mean \pm SE. Statistically significant differences among groups were assessed with ANOVA (with the Fisher post hoc least significant difference test), with values of $p < 0.05$ to sufficiently reject the null hypothesis for all analyses. In Figures 7 and S7, statistically significant differences among groups were assessed with t test ($n = 5$ –7 animals per group). All experiments were designed with matched control conditions within each experiment (minimum of five animals) to enable statistical comparison as paired samples and to obtain statistically significant data.

SUPPLEMENTAL INFORMATION

Supplemental Information includes seven figures and can be found with this article online at <http://dx.doi.org/10.1016/j.celrep.2014.03.025>.

ACKNOWLEDGMENTS

We thank Dr. Jeffrey A. Whitsett (Cincinnati Children's Hospital Medical Center) for generously providing *SP-C-rtTA/tetO-Cre* (line 2) mice and *CCSP-rtTA/tetO-Cre* (line 2) mice; Dr. Cheryl Walker (Texas A&M Health Science Center) for the generous gift of rat TSC2-null cells; Dr. Leslie A. Litzky (University of Pennsylvania) for help with tissue specimens from patients with BHD; Dr. Chang-Jiang Guo and Helen Abramova (Rutgers University) for excellent technical support; Ms. Sharmin Islam for preparing Figure S1A; and Mr. Nathan Tessema Ersumo for exceptional help with Figures 1 and 2, the graphical abstract, slider image, and technical assistance with the manuscript. This research was supported by the Intramural Research Program of NIH, Frederick National Laboratory for Cancer Research, and the Center for Cancer Research. This project has been funded in whole or in part with federal funds from the Frederick National Laboratory for Cancer Research, NIH, under contract HHSN261200800001E. The content of this publication does not necessarily reflect the views or policies of the DHHS, nor does mention of trade names, commercial products, or organizations imply endorsement by the US Government. This work was supported by NIH/NHLBI R01 HL110551 (to V.P.K.) and the Myrovlytis Trust (to S.-B.H. and V.P.K.).

Received: September 13, 2013

Revised: January 30, 2014

Accepted: March 10, 2014

Published: April 10, 2014

REFERENCES

Atochina-Vasserman, E.N., Bates, S.R., Zhang, P., Abramova, H., Zhang, Z., Gonzales, L., Tao, J.Q., Gochoico, B.R., Gahl, W., Guo, C.J., et al. (2011). Early alveolar epithelial dysfunction promotes lung inflammation in a mouse

model of Hermansky-Pudlak syndrome. *Am. J. Respir. Crit. Care Med.* **184**, 449–458.

Baba, M., Hong, S.B., Sharma, N., Warren, M.B., Nickerson, M.L., Iwamatsu, A., Esposito, D., Gillette, W.K., Hopkins, R.F., 3rd, Hartley, J.L., et al. (2006). Folliculin encoded by the BHD gene interacts with a binding protein, FNIP1, and AMPK, and is involved in AMPK and mTOR signaling. *Proc. Natl. Acad. Sci. USA* **103**, 15552–15557.

Baba, M., Furihata, M., Hong, S.B., Tessarollo, L., Haines, D.C., Southon, E., Patel, V., Igarashi, P., Alvord, W.G., Leighty, R., et al. (2008). Kidney-targeted Birt-Hogg-Dube gene inactivation in a mouse model: Erk1/2 and Akt-mTOR activation, cell hyperproliferation, and polycystic kidneys. *J. Natl. Cancer Inst.* **100**, 140–154.

Barnes, P.J. (2010). Medicine. Neutrophils find smoke attractive. *Science* **330**, 40–41.

Barnes, E.A., Kenerson, H.L., Jiang, X., and Yeung, R.S. (2010). Tuberin regulates E-cadherin localization: implications in epithelial-mesenchymal transition. *Am. J. Pathol.* **177**, 1765–1778.

Birt, A.R., Hogg, G.R., and Dubé, W.J. (1977). Hereditary multiple fibrofolliculomas with trichodiscomas and acrochordons. *Arch. Dermatol.* **113**, 1674–1677.

Cash, T.P., Gruber, J.J., Hartman, T.R., Henske, E.P., and Simon, M.C. (2011). Loss of the Birt-Hogg-Dubé tumor suppressor results in apoptotic resistance due to aberrant TGF β -mediated transcription. *Oncogene* **30**, 2534–2546.

DiPaolo, B.C., and Margulies, S.S. (2012). Rho kinase signaling pathways during stretch in primary alveolar epithelia. *Am. J. Physiol. Lung Cell. Mol. Physiol.* **302**, L992–L1002.

Frisch, S.M., and Srean, R.A. (2001). Anokiis mechanisms. *Curr. Opin. Cell Biol.* **13**, 555–562.

Goncharova, E., Goncharov, D., Noonan, D., and Krymskaya, V.P. (2004). TSC2 modulates actin cytoskeleton and focal adhesion through TSC1-binding domain and the Rac1 GTPase. *J. Cell Biol.* **167**, 1171–1182.

Goncharova, E.A., Goncharov, D.A., Li, H., Pimtong, W., Lu, S., Khavin, I., and Krymskaya, V.P. (2011). mTORC2 is required for proliferation and survival of TSC2-null cells. *Mol. Cell. Biol.* **31**, 2484–2498.

Goncharova, E.A., Goncharov, D.A., Fehrenbach, M., Khavin, I., Ducka, B., Hino, O., Colby, T.V., Merrilees, M.J., Haczk, A., Albelda, S.M., and Krymskaya, V.P. (2012). Prevention of alveolar destruction and airspace enlargement in a mouse model of pulmonary lymphangiomyomatosis (LAM). *Sci. Transl. Med.* **4**, ra134.

Gupta, N., Seyama, K., and McCormack, F.X. (2013). Pulmonary manifestations of Birt-Hogg-Dubé syndrome. *Fam. Cancer* **12**, 387–396.

Guttentag, S.H., Akhtar, A., Tao, J.Q., Atochina, E., Rusiniak, M.E., Swank, R.T., and Bates, S.R. (2005). Defective surfactant secretion in a mouse model of Hermansky-Pudlak syndrome. *Am. J. Respir. Cell Mol. Biol.* **33**, 14–21.

Haczku, A., Atochina, E.N., Tomer, Y., Cao, Y., Campbell, C., Scanlon, S.T., Russo, S.J., Enhorning, G., and Beers, M.F. (2002). The late asthmatic response is linked with increased surface tension and reduced surfactant protein B in mice. *Am. J. Physiol. Lung Cell. Mol. Physiol.* **283**, L755–L765.

Hardie, D.G. (2011). AMP-activated protein kinase: an energy sensor that regulates all aspects of cell function. *Genes Dev.* **25**, 1895–1908.

Hasumi, H., Baba, M., Hong, S.B., Hasumi, Y., Huang, Y., Yao, M., Valera, V.A., Linehan, W.M., and Schmidt, L.S. (2008). Identification and characterization of a novel folliculin-interacting protein FNIP2. *Gene* **415**, 60–67.

Hasumi, Y., Baba, M., Ajima, R., Hasumi, H., Valera, V.A., Klein, M.E., Haines, D.C., Merino, M.J., Hong, S.B., Yamaguchi, T.P., et al. (2009). Homozygous loss of BHD causes early embryonic lethality and kidney tumor development with activation of mTORC1 and mTORC2. *Proc. Natl. Acad. Sci. USA* **106**, 18722–18727.

Hasumi, H., Baba, M., Hasumi, Y., Huang, Y., Oh, H., Hughes, R.M., Klein, M.E., Takikita, S., Nagashima, K., Schmidt, L.S., and Linehan, W.M. (2012). Regulation of mitochondrial oxidative metabolism by tumor suppressor FLCN. *J. Natl. Cancer Inst.* **104**, 1750–1764.

- Henson, P.M., and Tuder, R.M. (2008). Apoptosis in the lung: induction, clearance and detection. *Am. J. Physiol. Lung Cell. Mol. Physiol.* *294*, L601–L611.
- Hong, S.B., Oh, H., Valera, V.A., Stull, J., Ngo, D.T., Baba, M., Merino, M.J., Linehan, W.M., and Schmidt, L.S. (2010). Tumor suppressor FLCN inhibits tumorigenesis of a FLCN-null renal cancer cell line and regulates expression of key molecules in TGF-beta signaling. *Mol. Cancer* *9*, 160.
- Hwang, Y.P., and Jeong, H.G. (2010). Metformin blocks migration and invasion of tumour cells by inhibition of matrix metalloproteinase-9 activation through a calcium and protein kinase Calpha-dependent pathway: phorbol-12-myristate-13-acetate-induced/extracellular signal-regulated kinase/activator protein-1. *Br. J. Pharmacol.* *160*, 1195–1211.
- Jansen, M., Ten Klooster, J.P., Offerhaus, G.J., and Clevers, H. (2009). LKB1 and AMPK family signaling: the intimate link between cell polarity and energy metabolism. *Physiol. Rev.* *89*, 777–798.
- Klymenova, E., Ibraghimov-Beskrovnaya, O., Kugoh, H., Everitt, J., Xu, H., Kiguchi, K., Landes, G., Harris, P., and Walker, C. (2001). Tuberlin-dependent membrane localization of polycystin-1: a functional link between polycystic kidney disease and the TSC2 tumor suppressor gene. *Mol. Cell* *7*, 823–832.
- Lee, Y.M., Lee, J.O., Jung, J.H., Kim, J.H., Park, S.H., Park, J.M., Kim, E.K., Suh, P.G., and Kim, H.S. (2008). Retinoic acid leads to cytoskeletal rearrangement through AMPK-Rac1 and stimulates glucose uptake through AMPK-p38 MAPK in skeletal muscle cells. *J. Biol. Chem.* *283*, 33969–33974.
- Liu, C., Liang, B., Wang, Q., Wu, J., and Zou, M.H. (2010). Activation of AMP-activated protein kinase alpha1 alleviates endothelial cell apoptosis by increasing the expression of anti-apoptotic proteins Bcl-2 and survivin. *J. Biol. Chem.* *285*, 15346–15355.
- Liu, W., Chen, Z., Ma, Y., Wu, X., Jin, Y., and Hou, S. (2013). Genetic characterization of the *Drosophila* birt-hogg-dubé syndrome gene. *PLoS ONE* *8*, e65869.
- Makowski, L., and Hayes, D.N. (2008). Role of LKB1 in lung cancer development. *Br. J. Cancer* *99*, 683–688.
- Morizane, Y., Thanos, A., Takeuchi, K., Murakami, Y., Kayama, M., Trichonas, G., Miller, J., Foretz, M., Viollet, B., and Vavvas, D.G. (2011). AMP-activated protein kinase suppresses matrix metalloproteinase-9 expression in mouse embryonic fibroblasts. *J. Biol. Chem.* *286*, 16030–16038.
- Mouded, M., Egea, E.E., Brown, M.J., Hanlon, S.M., Houghton, A.M., Tsai, L.W., Ingenito, E.P., and Shapiro, S.D. (2009). Epithelial cell apoptosis causes acute lung injury masquerading as emphysema. *Am. J. Respir. Cell Mol. Biol.* *41*, 407–414.
- Nakano, A., Kato, H., Watanabe, T., Min, K.D., Yamazaki, S., Asano, Y., Seguchi, O., Higo, S., Shintani, Y., Asanuma, H., et al. (2010). AMPK controls the speed of microtubule polymerization and directional cell migration through CLIP-170 phosphorylation. *Nat. Cell Biol.* *12*, 583–590.
- Nickerson, M.L., Warren, M.B., Toro, J.R., Matrosova, V., Glenn, G., Turner, M.L., Duray, P., Merino, M., Choyke, P., Pavlovich, C.P., et al. (2002). Mutations in a novel gene lead to kidney tumors, lung wall defects, and benign tumors of the hair follicle in patients with the Birt-Hogg-Dubé syndrome. *Cancer Cell* *2*, 157–164.
- Perl, A.K., Zhang, L., and Whitsett, J.A. (2009). Conditional expression of genes in the respiratory epithelium in transgenic mice: cautionary notes and toward building a better mouse trap. *Am. J. Respir. Cell Mol. Biol.* *40*, 1–3.
- Ramirez, M.I., Millien, G., Hinds, A., Cao, Y., Seldin, D.C., and Williams, M.C. (2003). T1 α , a lung type I cell differentiation gene, is required for normal lung cell proliferation and alveolus formation at birth. *Dev. Biol.* *256*, 61–72.
- Schmidt, L.S. (2004). Birt-Hogg-Dubé syndrome, a genodermatosis that increases risk for renal carcinoma. *Curr. Mol. Med.* *4*, 877–885.
- Schmidt, L.S., Warren, M.B., Nickerson, M.L., Weirich, G., Matrosova, V., Toro, J.R., Turner, M.L., Duray, P., Merino, M., Hewitt, S., et al. (2001). Birt-Hogg-Dubé syndrome, a genodermatosis associated with spontaneous pneumothorax and kidney neoplasia, maps to chromosome 17p11.2. *Am. J. Hum. Genet.* *69*, 876–882.
- Sebbagh, M., Santoni, M.J., Hall, B., Borg, J.P., and Schwartz, M.A. (2009). Regulation of LKB1/STRAD localization and function by E-cadherin. *Curr. Biol.* *19*, 37–42.
- Shapiro, S.D., and Ingenito, E.P. (2005). The pathogenesis of chronic obstructive pulmonary disease: advances in the past 100 years. *Am. J. Respir. Cell Mol. Biol.* *32*, 367–372.
- Suki, B., Lutchen, K.R., and Ingenito, E.P. (2003). On the progressive nature of emphysema: roles of proteases, inflammation, and mechanical forces. *Am. J. Respir. Crit. Care Med.* *168*, 516–521.
- Takagi, Y., Kobayashi, T., Shiono, M., Wang, L., Piao, X., Sun, G., Zhang, D., Abe, M., Hagiwara, Y., Takahashi, K., and Hino, O. (2008). Interaction of folliculin (Birt-Hogg-Dubé gene product) with a novel Fnipl1-like (Fnipl/Fnipl2) protein. *Oncogene* *27*, 5339–5347.
- Taliaferro-Smith, L., Nagalingam, A., Zhong, D., Zhou, W., Saxena, N.K., and Sharma, D. (2009). LKB1 is required for adiponectin-mediated modulation of AMPK-S6K axis and inhibition of migration and invasion of breast cancer cells. *Oncogene* *28*, 2621–2633.
- van Slegtenhorst, M., Khabibullin, D., Hartman, T.R., Nicolas, E., Kruger, W.D., and Henske, E.P. (2007). The Birt-Hogg-Dubé and tuberous sclerosis complex homologs have opposing roles in amino acid homeostasis in *Schizosaccharomyces pombe*. *J. Biol. Chem.* *282*, 24583–24590.
- Vocke, C.D., Yang, Y., Pavlovich, C.P., Schmidt, L.S., Nickerson, M.L., Torres-Cabala, C.A., Merino, M.J., Walther, M.M., Zbar, B., and Linehan, W.M. (2005). High frequency of somatic frameshift BHD gene mutations in Birt-Hogg-Dubé-associated renal tumors. *J. Natl. Cancer Inst.* *97*, 931–935.
- Xu, X., Jin, D., Durgan, J., and Hall, A. (2013). LKB1 controls human bronchial epithelial morphogenesis through p114RhoGEF-dependent RhoA activation. *Mol. Cell. Biol.* *33*, 2671–2682.
- Zhang, L., Li, J., Young, L.H., and Caplan, M.J. (2006). AMP-activated protein kinase regulates the assembly of epithelial tight junctions. *Proc. Natl. Acad. Sci. USA* *103*, 17272–17277.
- Zheng, B., and Cantley, L.C. (2007). Regulation of epithelial tight junction assembly and disassembly by AMP-activated protein kinase. *Proc. Natl. Acad. Sci. USA* *104*, 819–822.